Pergamon

Int. J. Heat Mass Transfer. Vol. 39, No. 7, pp. 1395–1406, 1996

0017–9310/96 $15.00 + 0.00

0017–9310(95)00216–2

Local jet impingement boiling heat transfer

D. H. WOLF†, F. P. INCROPERA and R. VISKANTA

Heat Transfer Laboratory, School of Mechanical Engineering, Purdue University, West Lafayette, IN 47907, U.S.A.

(*Received* 25 *July* 1994 *and in final form* 1 *June* 1995)

Abstract—This study focuses on some of the fundamental issues that influence boiling heat transfer to a free-surface, planar jet of water. Local boiling curves are presented at several streamwise distances from the stagnation line, while streamwise distributions of the surface temperature and convection coefficient are presented for representative heat fluxes. The position downstream of the stagnation line strongly influences heat transfer in the single-phase convection regime, has no appreciable effect on fully-developed nucleate boiling, but does influence the extent of the partial boiling regime. The effect of jet velocity on heat transfer is most pronounced in the single-phase and partial boiling regimes, where convective transport is dominated by the hydrodynamics of the bulk flow, and not by evaporation or bubble motion. Within the fully-developed boiling regime, the convective transport is dominated by evaporation and intense mixing induced by bubbles leaving the surface, and heat transfer is insensitive to jet velocity.

1. INTRODUCTION

For many years cooling by free-surface, liquid jets has been important in metal processing, and more recently it has been identified as a useful option for dissipating the high heat fluxes associated with applications such as very large scale integrated circuits and neutron beam dumping in fusion reactors. Sizable, efficient (in terms of liquid consumption), and controlled cooling play important roles in each of these applications. As it pertains to surface temperature uniformity, controlled cooling is often the most important consideration. This is true for microelectronics, where small temperature gradients across the chip surface can result in component failure.

Because of the attractiveness of jet impingement cooling for high-heat flux applications, numerous studies have been performed for both single- and two-phase conditions. Jet impingement boiling is distinguished by its ability to dissipate heat fluxes at the high end of the cooling spectrum, and due to the large range and magnitude of heat fluxes accompanying only small changes in the surface temperature, nucleate boiling is the desired mode of heat transfer for many cooling applications.

Wolf *et al.* [1] prepared a comprehensive review of the jet impingement boiling literature, including all modes of boiling (nucleate, transition, film), jet configurations (free-surface, submerged, confined, plunging, wall), and nozzle geometries (circular, planar). They showed that the impingement, nucleate boiling literature focused primarily on jets with low subcooling ($\Delta T_{sub} \lesssim 20°C$) and spatially-averaged measurements. To date, only a few studies of *local* nucleate boiling have been reported for impinging flows.

Miyasaka and Inada [2] measured local temperature distributions along the back-surface of a 0.1 mm-thick platinum heater serving as the impingement surface for a planar, free-surface jet of water. As many as seven equally spaced thermocouples (spot welded to the heater) were used, spanning a total distance of approximately 5 mm in the streamwise direction. The thermocouples and heater were positioned symmetrically about the stagnation line, as well as 2 1/2 nozzle widths downstream to investigate the parallel-flow region of the jet. Data at the stagnation line showed little variation of the surface temperature (within 5°C) over the range of heat fluxes associated with nucleate boiling. Although measurements in the downstream, parallel flow-region of the jet showed little variation in the temperature (within 5°C) for large surface heat fluxes, significant variations developed (up to 40°C) at lower heat fluxes in proximity to boiling incipience. These findings should be viewed cautiously, however, since the spatial extent of the temperature measurements was small (5 mm) compared to the width of the nozzle (10 mm). Hence, the reported local measurements comprised only a fraction of the total area beneath the jet. With respect to the stagnation line and the location which was 2 1/2 nozzle widths downstream, the fully-developed boiling curves were nearly coincident for the velocities investigated (3.2 and 15.3 m s^{-1}).

† Current address: Owens-Corning Science and Technology Center, 2790 Columbus Road, Granville, OH 43023, U.S.A.

NOMENCLATURE

A_n	nozzle cross sectional area
AR	aspect ratio of a rectangular channel (nozzle)
D_h	hydraulic diameter
E_T	total EMF applied to the heater between the voltage probes
g	gravitational acceleration
h	local convection heat transfer coefficient $(q''/[T_w - T_f])$
H	nozzle-to-surface spacing
k_f	thermal conductivity of the liquid
L	axial length of the heater between voltage probes
Pr	Prandtl number
q''	surface heat flux
$\dot{Q}$	volumetric flow rate
T_f	liquid temperature
T_m	local measured temperature on the dry side of the heated surface
T_{sat}	saturation temperature
T_w	local temperature on the wet side of the heated surface
$\bar{V}_j$	mass-averaged jet velocity at a distance y from the nozzle exit $(\bar{V}_n^2 + 2gy)^{1/2}$
$\bar{V}_n$	mass-averaged jet velocity at the nozzle discharge
w_j	jet width at a distance y from the nozzle exit $(w_n \bar{V}_n / \bar{V}_j)$
w_n	nozzle width
x	streamwise distance from the stagnation line.

Greek symbols

ΔT_f	temperature difference between the wall and free-stream $(T_w - T_f)$
ΔT_{sat}	wall superheat $(T_w - T_{sat})$
ΔT_{sub}	subcooling $(T_{sat} - T_f)$
γ	heater thickness
ν	kinematic viscosity
ρ_e	electrical resistivity.

Although Kamata *et al.* [3, 4] did not report a local temperature distribution along the surface, they compared boiling curves at radial positions of 0 and 5 mm for a circular, confined jet of saturated water ($d = 2.2$ mm). In part one of that investigation [3], a circular plate was attached to the nozzle exit and was parallel to the heater surface. Clearances between the nozzle-plate and heater were kept small (0.3–0.6 mm), and the 20 mm diameter of the confinement area was the same as that of the heater. For this flow geometry, the nucleate boiling curve was independent of the radial position (0 or 5 mm). Part two of the investigation [4] employed the same nozzle arrangement, but with the addition of a 0.2 mm brim around the circumference of the nozzle-plate (between the nozzle-plate and heated surface) to prevent stratification of the liquid and vapor at high heat fluxes. With the same nozzle-to-surface spacing, the nucleate boiling heat transfer at the stagnation point was indistinguishable from that of the brimless nozzle-plate [3]. However, differences existed between results obtained at radial distances of 0 and 5 mm for the brimmed nozzle-plate. For a fixed heat flux, the surface temperature at a radial distance of 5 mm was approximately 5–10°C higher than at the stagnation point.

Sano *et al.* [5], conducting transient experiments, reported nucleate boiling data at nine different streamwise locations ($0 \leqslant x \leqslant 56$ mm) for a free-surface, planar jet of saturated water (the nozzle dimension was not provided). No effect of streamwise distance on the nucleate boiling curve was evident.

Vader *et al.* [6] provided the most comprehensive investigation of local nucleate boiling for an impinging jet. They obtained local temperature measurements from the stagnation line to a downstream distance of up to 14 jet widths for a planar, free-surface jet of water. Surface temperatures were inferred from measurements on the rear of the heater and, for prescribed conditions, revealed coexistence of single-phase convection and nucleate boiling at different locations along the surface. The surface temperature distribution, in conjunction with high-speed photographs of the boiling process, enabled delineation of important features of boundary layer development, including the effects of nucleate boiling. For the lower heat fluxes (0.25–0.75 MW m^{-2}), their data showed an increase in surface temperature with the streamwise coordinate as the thickness of the laminar boundary layer increases. In the vicinity of the temperature maximum, the boundary layer began a transition to turbulent flow and higher levels of mixing caused a decline in the surface temperature. The maximum in temperature (approximate boundary layer transition point) was seen to occur at smaller values of the streamwise coordinate as the surface heat flux was increased. The authors suggested that flow disturbances induced by vapor formation on the surface were sufficient to accelerate boundary layer transition, reducing the critical Reynolds number obtained under single-phase convection by as much as 75%. For moderate heat fluxes (1.00–1.23 MW m^{-2}), the data showed nucleate boiling to be present but to be limited to downstream portions of the surface, where the temperature distribution was nearly isothermal. With increasing heat flux beyond 1.45 MW m^{-2}, the entire surface experienced fully-developed nucleate boiling.

The work of Vader *et al.* showed the local coupling between flow hydrodynamics and boiling, which had not been acknowledged in prior impingement boiling

publications. However, because of experimental limitations, results were restricted to heat fluxes near boiling incipience and hence to a small region of the fully-developed nucleate boiling curve. The objective of this investigation is to determine the effect of hydrodynamic conditions on boiling at larger heat fluxes near the critical heat flux (CHF). In particular, interactions between flow hydrodynamics and nucleate boiling are considered for a planar, free-surface jet of water at boiling conditions ranging from incipience to CHF.

2. EXPERIMENTAL METHODS AND APPARATUS

The experimental system was designed to provide a nonintrusive measurement of the local temperature distribution along a planar, uniformly heated surface, while allowing control and measurement of the heat flux, jet temperature and average jet velocity. The experimental arrangement is shown schematically in Fig. 1. The temperature distribution, $T_m(x)$, on the lower (dry), well insulated surface of an electrically heated plate was measured with thermocouples located along the direction of flow. Measurement of the voltage difference across the plate (E_T), coupled with the geometry (L and γ) and electrical resistivity (ρ_e, evaluated at the average plate temperature), provided sufficient information to infer the surface heat flux by an expression of the form $q'' = E_T^2\gamma/\rho_e L^2$. The wall temperature distribution, $T_w(x)$, on the upper (wet) surface of the plate was obtained from a solution of the steady-state energy equation within the solid, where the measured temperature distribution and near-adiabatic state on the lower surface provided the needed boundary conditions.

The dimensions of the rectangular nozzle were 10.2 mm × 102 mm (D_h = 18.5 mm; AR = 10), with an axial length of 935 mm (50.6D_h; 92w_n). The fluid consisted of demineralized, deionized water, which could not be effectively degassed prior to experiments due to the large size of the flow loop. The jet descended

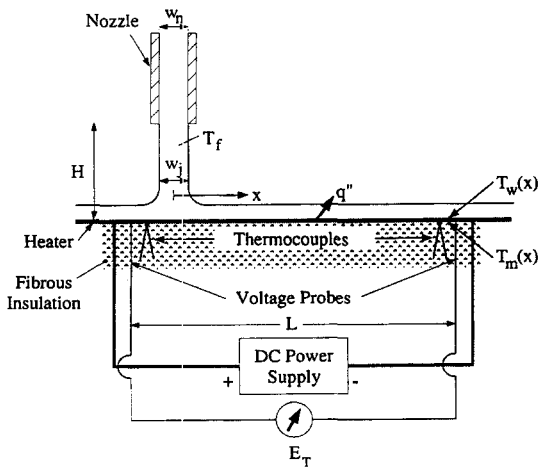

Fig. 1. Schematic of experimental apparatus.

normal to the heated surface over a distance (H) of 102 mm, and its temperature was held constant at 50°C (ΔT_{sub} = 50°C). The average jet velocity ($\bar{V}_j$) and width (w_j) were based on conditions at the nozzle exit ($\bar{V}_n$ and w_n) but were corrected for gravitational acceleration by expressions of the form $\bar{V}_j = (\bar{V}_n^2 + 2gH)^{1/2}$, $w_j = w_n(\bar{V}_n/\bar{V}_j)$, $\bar{V}_n = \dot{Q}/A_n$. The velocity profile across the width of the jet was measured and found to be nearly uniform at an axial distance from the discharge of 102 mm (the nozzle-to-surface spacing). More details regarding the velocity and turbulence characteristics of the jet may be found elsewhere [7–9].

The impingement surface was a uniformly heated strip of Ni–Cr–W–Mo alloy (Haynes Alloy 230) measuring 35.7 mm × 260 mm × 0.297 mm. The plate was subjected to direct current, Joulean heating by two power supplies positioned in series, with combined peak output of 30 kW (1500 A at 20 V). Two power lugs were soldered to the dry side of the plate where connections were made to the power supply.

Two types of experiments were conducted. One focused on measurement of the temperature distribution along the heated surface at several heat fluxes ($T_w(x)$ at six values of q''), while the other focused on measurement of the boiling curve at several surface locations ($q''(T_w)$ at five values of x). The measurements required the use of four different heater arrangements as shown in Fig. 2. The distance of the nozzle from the farthest downstream thermocouple is indicated, where the symbols T and V refer to locations of the thermocouples and voltage probes along the dry side of the heater. The local temperature distribution was measured with the arrangement of Fig. 2(a). The remaining configurations were used to measure boiling curves at locations of 10, 30, 50, 70 and 90 mm from the stagnation line.

Many studies of impingement boiling [10–15] have consistently observed the onset of film boiling to initiate at the perimeter of the heated surface, where convective transport is poorest. As the length of the heated surface increases, the critical heat flux decreases. The relationship between q''_{CHF} and the maximum heated length x for jet impingement systems is typically of the form $q''_{CHF} \sim x^{-n}$, where n is in the range $0.20 \lesssim n \lesssim 0.33$ [1]. Hence, to obtain a boiling curve at heat fluxes near CHF and at a surface location x from the stagnation line, the distance x must also be the longest heated section.

Consider, for example, the fully-instrumented heater shown in Fig. 2(a) (21 in-line thermocouples flanked on both ends by the positive and negative leads of the voltage probe). The nozzle is 90 mm upstream of the last thermocouple, and temperatures could be monitored at distances $x \leqslant 90$ mm from the stagnation line. However, boiling curves recorded at these locations would be limited to the maximum heat flux corresponding to the farthest downstream heated length of 90 mm. Therefore, in order to obtain boiling curves at selected locations of x = 10, 30, 50 and 70

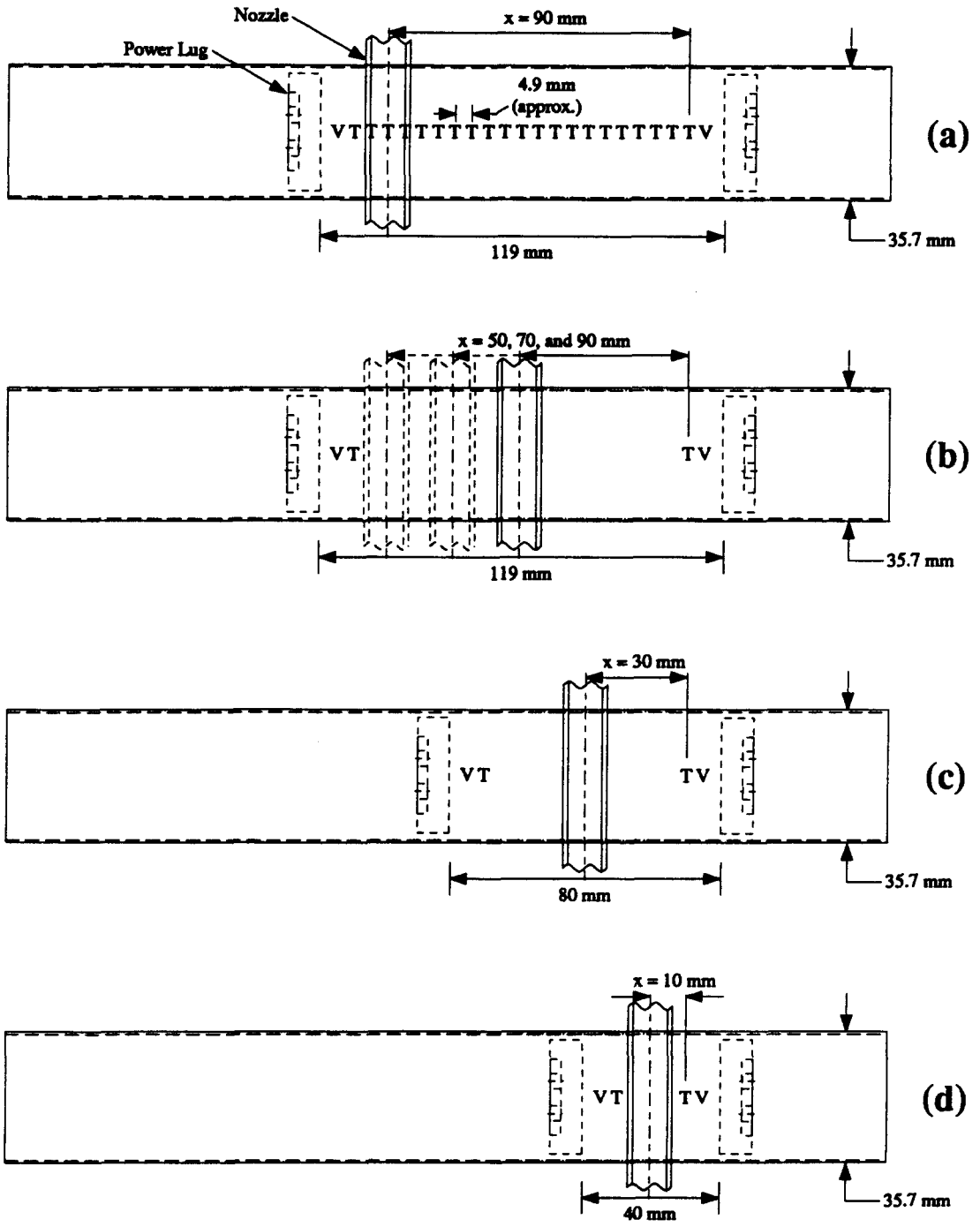

Fig. 2. Schematic diagram of heaters used in two-phase experiments: (a) fully-instrumented; and partially-instrumented used for maximum boiling distances of (b) $x = 50$, 70 and 90 mm, (c) $x = 30$ mm and (d) $x = 10$ mm.

mm, with heat fluxes near their respective maximum values, each location must also correspond to the longest heated length.

Measurements for $x = 50$, 70 and 90 mm were performed with the heater shown in Fig. 2(b) by changing the location of the nozzle relative to the thermocouple. However, experiments could not be conducted for $x \leqslant 50$ mm, since that location was approximately central to the total heated length. The configurations of Figs. 2(c) and (d) were used for the 30 and 10 mm downstream locations, respectively. The heater surface was treated by a vapor blasting process in which a mixture of water and abrasive grit (325 mesh silica-based material) is delivered to the surface by a high speed jet of air. This process produced a uniform and reproducible surface finish with a peak in the pore size distribution believed to be near 15 μm [6].

Thermocouple (chromel–alumel of diameter 0.127 mm) and voltage leads (copper of diameter 0.127 mm) were welded to the heater surface to ensure intimate contact. Each of the electrically insulated leads from a particular thermocouple departed from the bead in the spanwise direction and was epoxied to the surface to provide structural support and to inhibit heat losses along the wire. The thermocouple readings were corrected for the EMF induced by contact with a current-carrying element. Details of this correction are discussed elsewhere [7, 16].

The analysis of uncertainties was performed in accordance with the method suggested by Kline and McClintock [17] and Moffat [18], and details are provided by Wolf [7]. Overall uncertainties are based on the root-sum-square of the precision and bias limits and are: surface heat flux (q''), $\pm 2\%$; surface temperature (T_w), $\pm 2°C$; convection coefficient (h), $\pm 7\%$; average jet velocity ($\bar{V}_j$), $\pm 2\%$.

3. EXPERIMENTAL RESULTS AND DISCUSSION

Results are presented for the variation of the surface temperature T_w with heat flux q'' at several distances downstream of the stagnation line, as well as for streamwise distributions of the surface temperature and convection coefficient at several heat fluxes. The test matrix included variations in the jet velocity ($2 \leqslant \bar{V}_j \leqslant 5\ \mathrm{m\ s^{-1}}$), streamwise distance from the stagnation line ($10 \leqslant x \leqslant 90$ mm), and heat flux ($0.25 \leqslant q'' \leqslant 6.34\ \mathrm{MW\ m^{-2}}$).

At locations 10, 30, 50, 70 and 90 mm downstream of the stagnation line, the surface temperature T_w was measured in response to incremental variations in the heat flux. The local boiling results are presented in two ways: (1) heat flux q'' as a function of either the wall superheat ΔT_{sat} or the difference between the surface and free-stream fluid temperatures ΔT_f, and (2) convection heat transfer coefficient h as a function of either the wall superheat or the heat flux. Each format provides unique information about the local heat transfer.

To establish a fundamental understanding of the interaction between single-phase convection and boiling at a specific location on the surface, this section begins by analyzing the low ($\bar{V}_j = 2\ \mathrm{m\ s^{-1}}$) and high velocity ($\bar{V}_j = 5\ \mathrm{m\ s^{-1}}$) data at $x = 90$ mm. These results, typical of those at the other locations, are shown in Figs. 3(a) and (b), with the heat flux q'' plotted as a function of wall superheat, $\Delta T_{sat} = T_w - T_{sat}$, and the difference between the surface and free-stream temperatures, $\Delta T_f = T_w - T_f$, respectively. With boiling, energy transport is driven by ΔT_{sat} and is approximately independent of T_f. For single-phase convection, however, energy transport is driven by ΔT_f, which is related to the heat flux by Newton's law of cooling, $q'' = h\Delta T_f$. Hence, for fixed hydrodynamic conditions (fixed h), q'' and ΔT_f are linearly related. This linear relationship (slope of about unity on a log–log plot) is evident in Fig. 3(b) ($\Delta T_f \lesssim 55°C$ for $\bar{V}_j = 2\ \mathrm{m\ s^{-1}}$ and $\Delta T_f \lesssim 65°C$ for $\bar{V}_j = 5\ \mathrm{m\ s^{-1}}$), where heat transfer is by single-phase convection. In Fig. 4 the data of Fig. 3 are plotted in terms of the convection coefficient h ($q''/\Delta T_f$), where the dependence on ΔT_f or ΔT_{sat} is shown in Fig. 4(a) and the dependence on heat flux in (b). This format clearly identifies the modes of single-phase convection, partial nucleate boiling and fully-developed nucleate boiling.

For single-phase impingement heat transfer, h is a function of the bulk flow conditions (velocity, turbulence and velocity gradient), the characteristic dimension of the system (w_j), and the thermophysical properties (k_f, ν and Pr). Although the heat flux and temperature difference can have a small influence on the convection coefficient through their effects on thermophysical properties, there is no direct dependence on either q'' or ΔT_f. Hence, in the regions of Figs. 4(a) and (b) where h is nearly independent of the temperature difference and heat flux, heat transfer is by single-phase convection.

The low-velocity results show that at $\Delta T_f \approx 55°C$ ($T_w \approx 105°C$), the slope of the boiling curve in Fig. 3(b) begins to increase, as does the value of the convection coefficient in Fig. 4(a). The surface temperature of approximately 105°C marks the onset of nucleate boiling (ONB), where evaporation is initiated and discrete bubbles begin to detach from the surface, enhancing local fluid motion and heat transfer. For $55 \lesssim \Delta T_f \lesssim 80°C$, partial nucleate boiling exists with vapor generation limited to a small population of bubbles and the bulk flow continuing to strongly influence convection heat transfer from the surface. However, bubble-enhanced mixing and latent heat effects augment cooling by the bulk flow, yielding convection coefficients that exceed those for single-phase convection.

At $\Delta T_f \approx 80°C$ in Fig. 3(b) or $\Delta T_{sat} \approx 30°C$ in Fig. 3(a), the slope of the low-velocity boiling curve increases a second time, but much more precipitously. The same trends are evident for the corresponding convection coefficient in Fig. 4. At these elevated temperatures, boiling becomes fully developed, as the bubble density and size increase, and heat transfer is

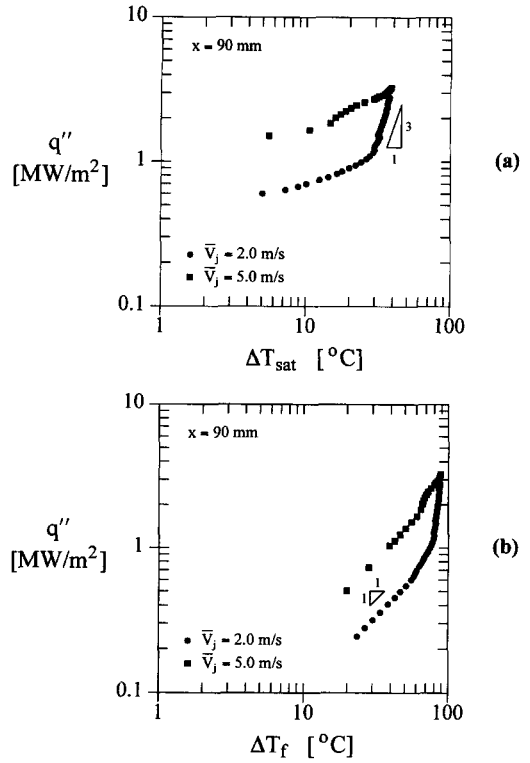

Fig. 3. Boiling curves for $\bar{V}_j = 2.0$ m s^{-1} and 5.0 m s^{-1} at $x = 90$ mm presented in terms of: (a) $\Delta T_{sat} = T_w - T_{sat}$ and (b) $\Delta T_f = T_w - T_f$.

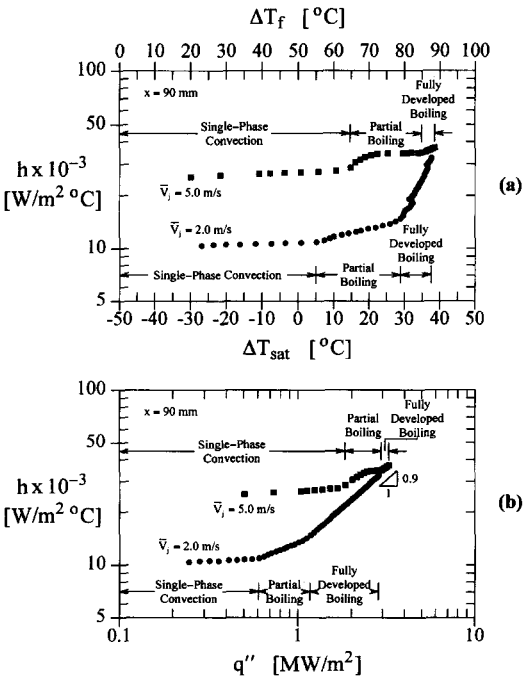

Fig. 4. Convection coefficients for $\bar{V}_j = 2.0$ m s^{-1} and 5.0 m s^{-1} at $x = 90$ mm as a function of: (a) ΔT_{sat} and ΔT_f and (b) q''.

largely the result of the latent heat of vapor generation and bubble departure from the surface.

By contrast, the high-velocity ($\bar{V}_j = 5$ m s^{-1}) data for $x = 90$ mm show that, except for the single-phase convection region, the overall shape of the boiling curve and the variation in the convection coefficient are markedly different from the low-velocity results. For example, the partial boiling regime for the low-velocity case exhibits a monotonic increase in the convection coefficient of approximately 35% with increasing surface temperature over its entire span of nearly 25°C ($5 \lesssim \Delta T_{sat} \lesssim 30$°C). In the high-velocity, partial boiling regime, however, the convection coefficient rises approximately 20% within the first 5°C ($15 \lesssim \Delta T_{sat} \lesssim 20$°C) and then maintains a nearly constant value over the last 15°C of the partial boiling regime ($20 \lesssim \Delta T_{sat} \lesssim 35$°C).

Although only conjecture, the foregoing difference in the partial boiling regime may be the result of differences in momentum between the free-stream flows of the low- and high-velocity jets. Heat transfer augmentation in this regime over single-phase convection is a combination of the latent heat liberated in the generation of vapor and the enhanced levels of mixing that accompany a bubble ejecting from the surface. In a low-velocity bulk flow, a bubble rising from the surface could possess sufficient momentum to escape the thermal boundary layer and induce mixing of the cooler, free-stream fluid with the warmer fluid close to the wall, thereby increasing heat transfer above the contributions derived from the latent heat. However, in a high-velocity bulk flow, a bubble departing from the surface is less likely to escape the thermal boundary layer and more likely to be dragged along the wall, thereby precluding the entrainment of relatively cold fluid from the free-stream. This behavior is particularly likely for the partial boiling regime, where the bubble population is typically low [19].

The low- and high-velocity convection coefficients (Fig. 4) exhibit a strong dependence on jet velocity in the single-phase convection and partial boiling regimes. This behavior is expected, since these regimes are dominated by bulk flow hydrodynamics and not by bubble motion. However, the convection coefficients are insensitive to the jet velocity in the fully-developed boiling regime, where convection is dominated by the intense mixing induced by bubbles leaving the surface and the energy absorbed in the phase change. Figures 3 and 4 show that the data in the fully-developed boiling regime for both velocities assume the same functional relationship, independent of velocity ($q'' \sim \Delta T_{sat}^3$ and $h \sim q''^{0.9}$, for example).

Figures 5 and 6 present the low velocity boiling curve and convection coefficient data, respectively, parameterized with respect to distance from the stagnation line. Similar results characterize the high velocity case [7]. Although the distance from the stagnation line, x, influences heat transfer in the single-phase convection regime, it has no appreciable effect

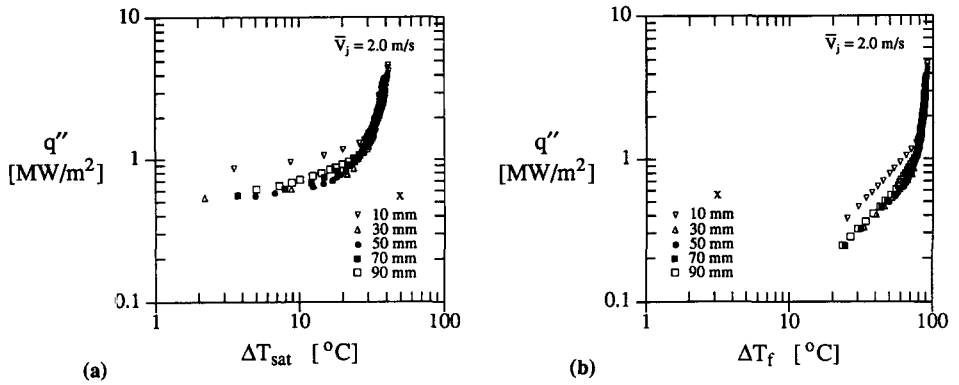

Fig. 5. Effect of distance from the stagnation line on the boiling curve for $\bar{V}_j = 2.0$ m s^{-1}; presented in terms of: (a) ΔT_{sat} and (b) ΔT_f.

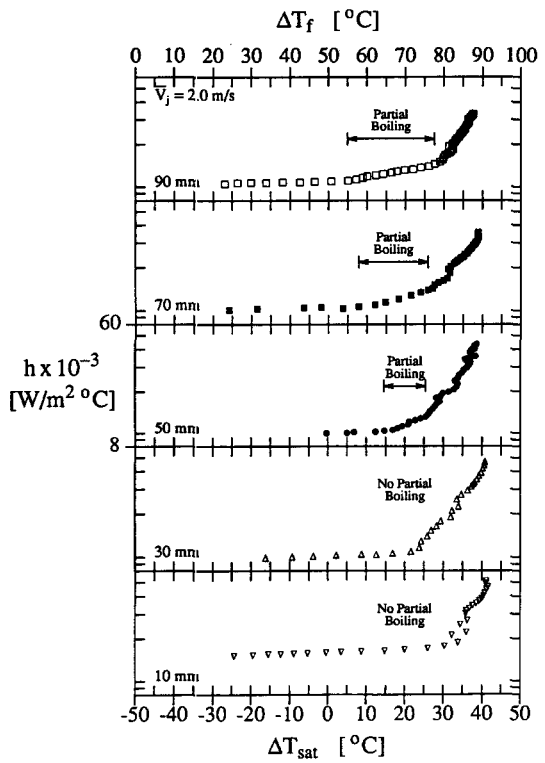

Fig. 6. Effect of distance from the stagnation line on the convection coefficient for $\bar{V}_j = 2.0$ m s^{-1}; presented in terms of ΔT_{sat} and ΔT_f. The ordinate for each of the five data sets spans the same range of $8000 \leqslant h \leqslant 60\,000$ W m^{-2}°C.

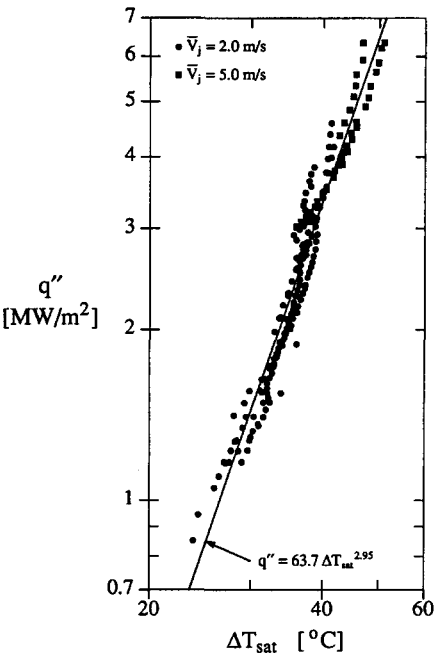

Fig. 7. Correlation of fully-developed boiling data ($q'' \sim \Delta T_{sat}$).

on fully-developed nucleate boiling. Within the single-phase regime, the convection coefficient (Fig. 6) at distances $x \geqslant 30$ mm is nearly constant (maximum 6% variation about 10 000 W m^{-2}°C) and approximately 33% less than the value at $x = 10$ mm ($\approx$15 000 W m^{-2}°C). The disparity, or lack there of, in h results from the influence of local hydrodynamic conditions on convective transport. Namely, the region $x = 10$ mm is close enough to the stagnation line to be strongly influenced by the enhanced heat transfer of jet impingement. At locations farther downstream ($x \gtrsim 30$ mm), the free-stream flow along the surface has fully accelerated and the effects of impingement, particularly augmented heat transfer, are no longer realized [16]. This will be more apparent later when the convection coefficient is presented as a function of streamwise distance.

The convection coefficients at the different locations have been plotted individually in Fig. 6 to accentuate some of their more subtle features. Note that the extent of the partial boiling regime decreases with decreasing x from a temperature interval of approximately 25°C at $x = 90$ mm to little or no partial boiling for $x \lesssim 30$ mm. Absence of partial boiling for $x \lesssim 30$ mm may be related to a corresponding delay in boiling incipience to wall superheats exceeding 20°C. Once nucleation is initiated at a particular site, it is plausible that these higher wall temperatures (and heat fluxes), coupled with mixing of the departing

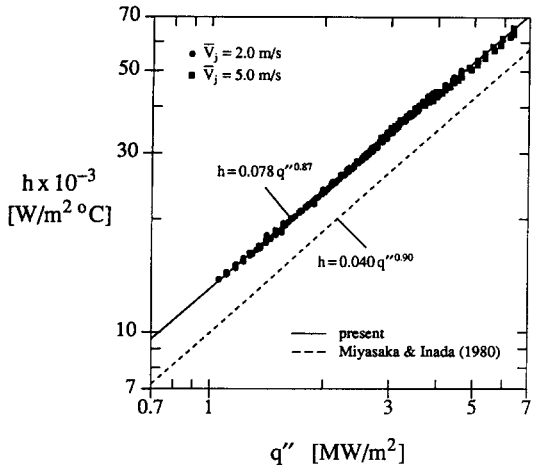

Fig. 8. Correlation of fully-developed boiling data ($h \sim q''$).

bubbles, are sufficient to induce vigorous boiling at many adjacent nucleation sites.

A correlation of $q''(\Delta T_{sat})$ for the fully-developed boiling regime was obtained from a least-squares fit of all fully-developed boiling data, independent of velocity or position (190 data in all). It is of the form

$$q'' = 63.7\Delta T_{sat}^{2.95} \tag{1}$$

where q'' and ΔT_{sat} have units of W m^{-2} and °C, respectively, and represents data for $23 \leqslant \Delta T_{sat} \leqslant 51$°C. This expression correlated all of the data to within ±32% and had a 95%-confidence interval of ±21% (i.e. 19 out of 20 data lie within an interval of ±21% of the correlation). The correlation and the data are shown in Fig. 7.

A correlation of $h(q'')$ was also obtained by a least-squares fit of the fully-developed boiling data and corresponds to

$$h = 0.0782q''^{0.870} \tag{2}$$

where h and q'' have units of W m^{-2}°C and W m^{-2}, respectively. This expression represents data within the heat flux range $1.0 \leqslant q'' \leqslant 6.4$ MW m^{-2}, and it correlated all of the data to within ±4% with a 95%-confidence interval of ±3%. The correlation and the data are shown in Fig. 8, along with a correlation obtained by Miyasaka and Inada [2] at the stagnation line of a planar, free-surface jet of highly subcooled ($85 \leqslant \Delta T_{sub} \leqslant 110$°C) water. Although the exponent (~0.9) is consistent in both correlations, the constant of proportionality differs by nearly a factor of two. This discrepancy is largely the result of differences in subcooling, with $\Delta T_{sub} = 50$°C for this investigation.

A relationship between h and q'' may be inferred from the following, generic expression for fully-developed nucleate boiling

$$q'' = C\Delta T_{sat}^{n} \tag{3}$$

and from Newton's law of cooling

$$q'' = h(T_w - T_f) = h(\Delta T_{sat} + \Delta T_{sub}). \tag{4}$$

Equation (4) may be rearranged to solve for ΔT_{sat}, giving

$$\Delta T_{sat} = (q''/h) - \Delta T_{sub} \tag{5}$$

which may then be substituted into equation (3) and solved for h to yield

$$h = \frac{q''}{(q''/C)^{1/n} + \Delta T_{sub}}. \tag{6}$$

This expression reveals that h is a function of *both* q'' and ΔT_{sub}. For decreasing ΔT_{sub}, the convection coefficient increases monotonically for a fixed heat flux. Equation (6) also shows that the relationship between h and q'' is not truly linear on a log–log scale, as both equation (2) and Fig. 8 would suggest.

Figures 9 and 10 show surface temperature and convection coefficient distributions for $\bar{V}_j = 2.0$ m s^{-1}, with the dashed line in Fig. 9 representing the saturation temperature at atmospheric pressure. To assist in the interpretation of these distributions, the local convection coefficient data of Fig. 6 are re-plotted with the heat flux on the abscissa in Fig. 11, with the dashed lines corresponding to the specific heat fluxes in Figs. 9 and 10. High-speed photographs of the heated surface are presented in Fig. 12 to provide qualitative information pertaining to the location and intensity of boiling.

At the lowest heat flux of 0.25 MW m^{-2}, the surface temperatures in Fig. 9 are well below that of saturation, and heat transfer is by single-phase convection [16]. As shown in Fig. 11, the convection coefficient is approximately independent of heat flux at all surface locations where $q'' \lesssim 0.75$ MW m^{-2}, lending further support for single-phase convection only.

At 0.75 MW m^{-2}, heat transfer is still predominantly by single-phase convection, despite surface temperatures that exceed T_{sat} (Fig. 9). This result is apparent from the convection coefficient distribution (Fig. 10), which is only slightly greater than that corresponding to 0.25 MW m^{-2}. The small increase in h is due partly to the influence of surface temperature on the thermophysical properties [20] and partly to boiling incipience. Based on the local results shown in Fig. 11, incipience is likely to occur for heat fluxes near 0.75 MW m^{-2} at surface locations where $x \gtrsim 30$ mm. Moreover, close observation of the photograph corresponding to 0.75 MW m^{-2}, Figure 12(a), reveals the presence of vapor bubbles, albeit very limited, downstream of 30 mm [note the small bubbles (black dots) at 36, 43, 47, 59, 68 and 70 mm, as well as somewhat larger bubbles at 76 and 78 mm].

At 1.24 MW m^{-2}, the surface temperature exceeds that of saturation everywhere on the surface (Fig. 9); however, based on the convection coefficient distribution (Fig. 10), boiling appears to be confined to regions where $x \gtrsim 15$ mm. The local results given in Fig. 11 support this conclusion by showing incipience at $x = 10$ mm to occur for $q'' \approx 1.4$ MW m^{-2}. The photograph corresponding to 1.24 MW m^{-2} is shown

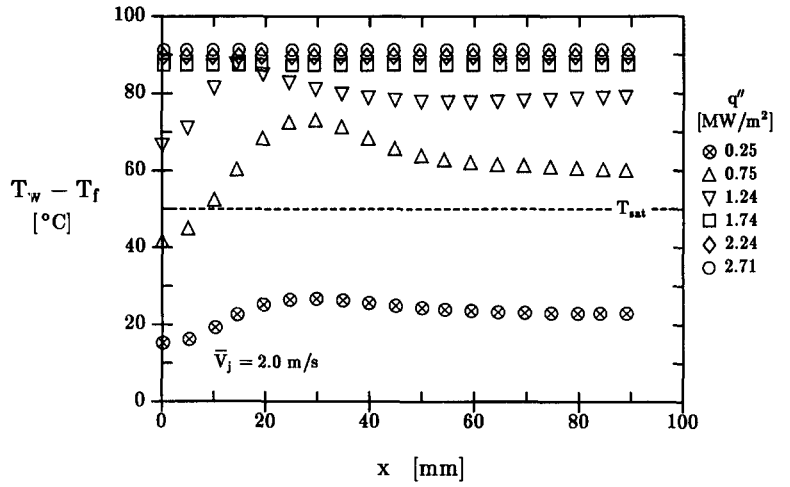

Fig. 9. Effect of heat flux on the surface temperature distribution for $\bar{V}_j = 2.0$ m s^{-1}.

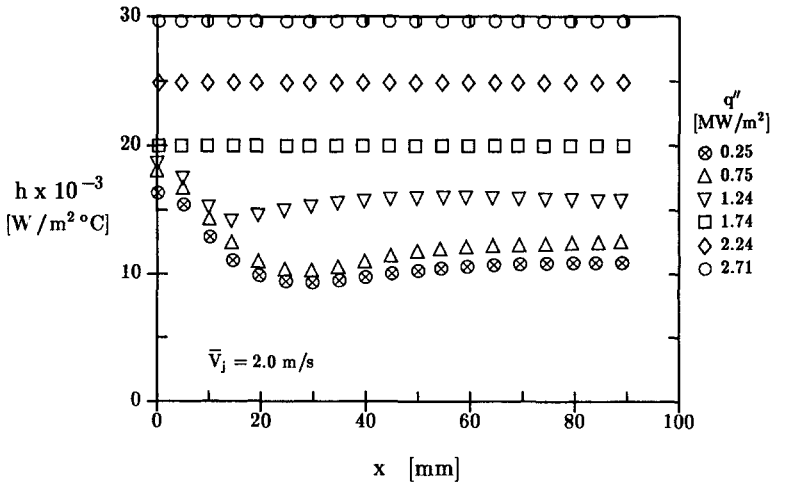

Fig. 10. Effect of heat flux on the convection coefficient distribution for $\bar{V}_j = 2.0$ m s^{-1}.

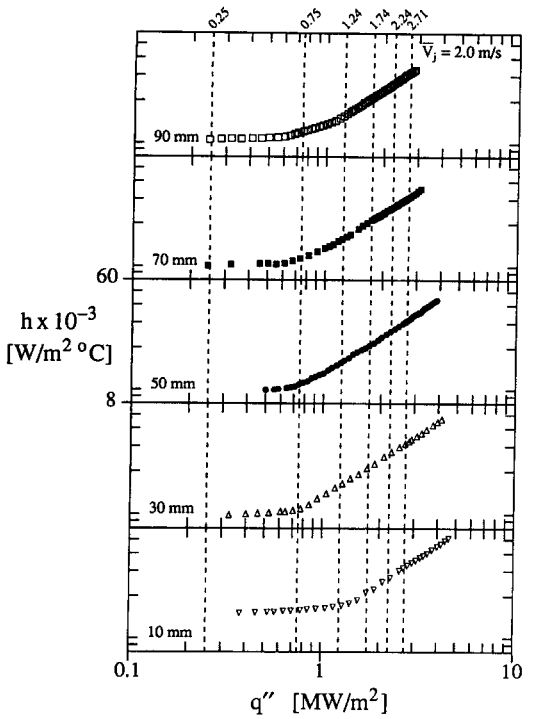

Fig. 11. Variation of the convection coefficient with heat flux for $\bar{V}_j = 2.0\ m\ s^{-1}$ and different surface locations. The dashed lines denote the heat fluxes shown in Figs. 9 and 10. The ordinate for each of the five data sets spans the same range of $8000 \leqslant h \leqslant 60\,000\ W\ m^{-2}°C$.

in Fig. 12(b). The bubble size and population are greater than those shown in Fig. 12(a) (0.75 MW m^{-2}), and bubbles may be seen over the entire surface, except within approximately 15 mm of the stagnation line, consistent with the quantitative results.

At heat fluxes in the range $1.74 \leqslant q'' \leqslant 2.71$ MW m^{-2}, the surface temperature and convection coefficient distributions are uniform (Figs. 9 and 10), indicating the presence of fully-developed nucleate boiling over the entire surface. Convection heat transfer associated with this mode of boiling is dominated by bubble-induced mixing and the latent energy of phase change, while the influence of free-stream hydrodynamics is essentially nil. Figures 12(c)–(e) show the photographs corresponding to the heat fluxes of 1.74, 2.24 and 2.71 MW m^{-2}, respectively. In each of the photographs, bubbles are evident at all surface locations, and the bubble population increases with heat flux.

The heat flux of 2.71 MW m^{-2} [Fig. 12(e)] is within 5% of the maximum heat flux at a location 90 mm downstream of the stagnation line. In the vicinity of 90 mm, Fig. 12(e) shows pronounced disturbances in the air–water interface which obstruct the view of the heater surface. The disturbances are probably induced by large quantities of vapor either approaching or penetrating the free surface. Vapor penetration through the interface of a free-surface jet has been reported by others near the critical or maximum heat flux [1]. Comparable results corresponding to $\bar{V}_j = 5.0\ m\ s^{-1}$ may be found elsewhere [7].

4. SUMMARY

Measurements were obtained for a planar, free-surface jet of subcooled ($\Delta T_{sub} = 50°C$) water impinging normal to a constant heat flux surface. Local boiling curves were obtained at several streamwise distances from the stagnation line, as were streamwise distributions of the surface temperature and convection coefficient for several heat fluxes.

By plotting the convection coefficient as a function of either the wall superheat or heat flux, the various modes of heat transfer (single-phase convection, partial nucleate boiling, and fully-developed nucleate boiling) were distinguished. For single-phase convection, h was shown to be a function of the bulk flow conditions only and to have no direct dependence on either q'' or ΔT_f. At surface temperatures in excess of saturation, the onset of nucleate boiling was identified by a marked increase in the convection coefficient, which continued to increase with increasing surface temperature (heat flux) throughout the partial boiling regime. The onset of fully-developed nucleate boiling was typically indicated by a second, much more precipitous, increase in the convection coefficient.

The streamwise distance from the stagnation line influenced heat transfer predominantly in the single-phase convection regime and had no appreciable effect on fully-developed nucleate boiling. However, surface location did influence the extent of the partial boiling regime. The range of wall temperatures encompassing the partial boiling regime decreased with decreasing distance from the stagnation line, shrinking from a wall temperature span of approximately 25°C at $x = 90$ mm to little or no partial boiling for $x \lesssim 30$ mm.

The effect of jet velocity on the heat transfer was most pronounced in the single-phase and partial boiling regimes, where convective transport is dominated by the hydrodynamics of the bulk flow and not by bubble motion. At the lower velocity ($\bar{V}_j = 2.0\ m\ s^{-1}$) the convection coefficient increased with increasing surface temperature throughout the partial boiling regime. However, for the higher velocity ($\bar{V}_j = 5.0\ m\ s^{-1}$), an initial rise in the convection coefficient with increasing ΔT_{sat} was followed by a much larger range of wall superheats for which the convection coefficient was nearly constant. In the fully-developed boiling regime, convection was dominated by the intense, bubble-induced mixing and latent heat effects, and heat transfer was independent of the jet velocity.

Acknowledgements—This work was supported by the National Science Foundation under grant numbers CTS-8912831 and CTS-9307232.

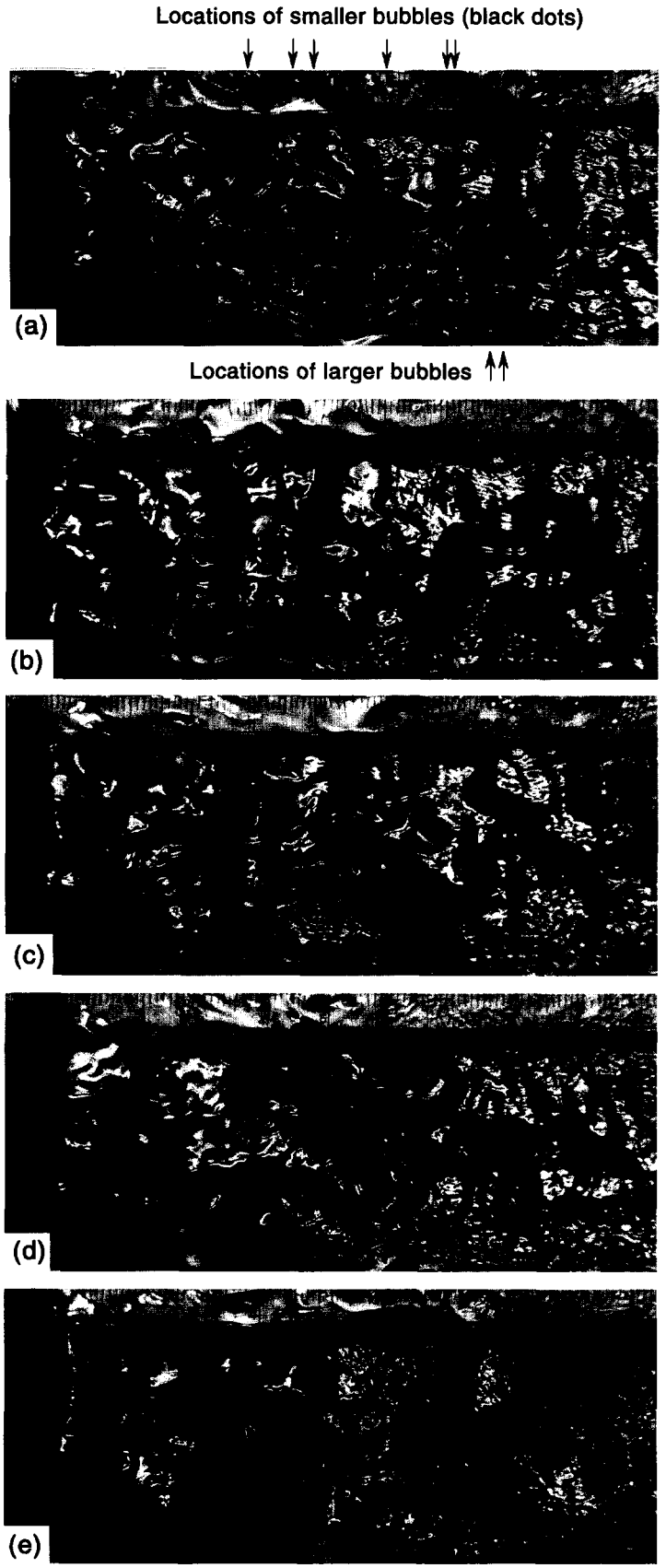

Fig. 12. Photographs of the boiling surface for $\bar{V}_j = 2.0$ m s^{-1} and $q'' =$: (a) 0.75 MW m^{-2}, (b) 1.24 MW m^{-2}, (c) 1.74 MW m^{-2}, (d) 2.24 MW m^{-2} and (e) 2.71 MW m^{-2}. The stagnation line is at the left edge of each photograph. A scale, numerated in centimeters, is positioned at the top of each photograph.

REFERENCES

1. D. H. Wolf, F. P. Incropera and R. Viskanta, Jet impingement boiling. In *Advances in Heat Transfer* (Edited by J. P. Hartnett *et al.*), Vol. 23, pp. 1–132. Academic Press, New York (1993).
2. Y. Miyasaka and S. Inada, The effect of pure forced convection on the boiling heat transfer between a two-dimensional subcooled water jet and a heated surface, *J. Chem. Engng Japan* **13,** 22–28 (1980).
3. T. Kamata, S. Kumagai and T. Takeyama, Boiling heat transfer to an impinging jet spurted into a narrow space—I. Space with an open end, *Heat Transfer—Jap. Res.* **17**(5), 71–80 (1988).
4. T. Kamata, S. Kumagai and T. Takeyama, Boiling heat transfer to an impinging jet spurted into a narrow space—II. Space with a limited end, *Heat Transfer—Jap. Res.* **17**(4), 1–11 (1988).
5. Y. Sano, R. Kubo, T. Kamata and S. Kumagai, Boiling heat transfer to an impinging jet in cooling a hot metal slab, *Proceedings of the 28th National Heat Transfer Symposium of Japan*, pp. 733–735 (1991) (in Japanese).
6. D. T. Vader, F. P. Incropera and R. Viskanta, Convective nucleate boiling on a heated surface cooled by an impinging, planar jet of water, *J. Heat Transfer* **114,** 152–160 (1992).
7. D. H. Wolf, Turbulent development in a free-surface jet and impingement boiling heat transfer, Ph.D. Thesis, Purdue University, West Lafayette, IN (1993).
8. D. H. Wolf, F. P. Incropera and R. Viskanta, Measurement of the turbulent flow field in a free-surface jet of water, *Exper. Fluids* **18,** 397–408 (1995).
9. D. H. Wolf, R. Viskanta and F. P. Incropera, Turbulence dissipation in a free-surface jet of water and its effect on local impingement heat transfer from a heated surface—I. Flow structure, *J. Heat Transfer* **117,** 85–94 (1995).
10. Y. Katto and M. Kunihiro, Study of the mechanism of burn-out in boiling system of high burn-out heat flux, *Bull. JSME* **16,** 1357–1366 (1973).
11. Y. Katto and K. Ishii, Burnout in a high heat flux boiling system with a forced supply of liquid through a plane jet, *Proceedings of the 6th International Heat Transfer Conference*, Vol. 1, FB-28, pp. 435–440 (1978).
12. M. Monde and Y. Katto, Burnout in a high heat-flux boiling system with an impinging jet, *Int. J. Heat Mass Transfer* **21,** 295–305 (1978).
13. M. Monde, Burnout heat flux in saturated forced convection boiling with an impinging jet, *Heat Transfer—Jap. Res.* **9**(1), 31–41 (1980).
14. C. F. Ma and A. E. Bergles, Boiling jet impingement cooling of simulated microelectronic chips. In *Heat Transfer in Electronic Equipment*—1983 (Edited by S. Oktay and A. Bar-Cohen), HTD-Vol. 28, pp. 5–12. ASME, New York (1983).
15. C. S. K. Cho and K. Wu, Comparison of burnout characteristics in jet impingement cooling and spray cooling, *Proceedings of the* 1988 *National Heat Transfer Conference* (Edited by H. R. Jacobs), HTD-96, Vol. 1, pp. 561–567. ASME, New York (1988).
16. D. H. Wolf, R. Viskanta and F. P. Incropera, Turbulence dissipation in a free-surface jet of water and its effect on local impingement heat transfer from a heated surface—II. Local heat transfer, *J. Heat Transfer* **117,** 95–103 (1995).
17. S. J. Kline and F. A. McClintock, Describing uncertainties in single-sample experiments, *Mech. Engng* **75,** 3–8 (1953).
18. R. J. Moffat, Describing the uncertainties in experimental results, *Exper. Thermal Fluid Sci.* **1,** 3–17 (1988).
19. J. G. Collier, *Convective Boiling and Condensation*, p. 156. McGraw-Hill, New York (1981).
20. D. T. Vader, F. P. Incropera and R. Viskanta, Local convective heat transfer from a heated surface to an impinging, planar jet of water, *Int. J. Heat Mass Transfer* **34,** 611–623 (1991).